Structure of NaF–TeO$_2$ glasses and glass-ceramics

E.F. El Agammy[a,*], H. Doweidar[a], K. El-Egili[a], R. Ramadan[b], Mariusz Jaremko[c], Abdul-Hamid Emwas[d]

[a] Glass Research Group, Physics Department, Faculty of Science, Mansoura University, Mansoura, 35516, Egypt
[b] Microwave and Dielectrics Department, Physics Division, National Research Centre, Dokki, 12311, Cairo, Egypt
[c] King Abdullah University of Science and Technology (KAUST), Biological and Environmental Science and Engineering (BESE), 23955-6900, Thuwal, Saudi Arabia
[d] King Abdullah University of Science and Technology (KAUST), Core Labs, Thuwal, Saudi Arabia

ARTICLE INFO

ABSTRACT

The structure of NaF–TeO$_2$ glasses and glass-ceramics has been studied by XRD, TEM, SEM, Raman and FTIR techniques. The results suggest that, for NaF ≤ 10 mol%, the entire NaF content enters the structure to convert TeO$_4$ units into TeO$_{3/2}$F and Na$^+$[TeO$_{3+1}$]$^-$ units. It has also been shown that NaF partially forms amorphous and/or crystalline phases for higher NaF content, where the relative concentration of each phase depends on the NaF content. SEM images show agglomerates of different sizes, which are discrete and spread within the structure. XRD revealed formation of crystalline Te$_2$O$_3$F$_2$ for NaF ≤ 50 mol%, and a dominant phase of crystalline NaF for NaF > 50 mol%. Raman and FTIR spectra have been analyzed to calculate the concentrations of the various structural units in glasses and glass-ceramics.

1. Introduction

Tellurite glasses are distinguished by high values of refractive index (usually larger than 2.0), wide infrared transmittance (expanded up to 6 μm), and good chemical durability [1–3]. As optical materials, oxyfluoride tellurite glass-ceramics have certain advantages, such as low phonon energy. The highest phonon energy in tellurite glasses (equivalent to ~ 750 cm^{-1}) is quite lower than that in borate- (~ 1400 cm^{-1}), phosphate- (~ 1300 cm^{-1}) and silicate glasses (~ 1100 cm^{-1}) [1,4]. They also have high optical transmittance, low melting temperature and high up-conversion efficiency [2,5–7].

Without a modifier and/or other types of glass formers, tellurium oxide cannot form a glass under normal conditions [8–12]. It is indicated that [13,14] TeO$_2$ glass consists of TeO$_4$ trigonal bipyramids (tbp's), with a lone pair of electrons occupying one of the equatorial sites. The connection between most of Te atoms is through vertices by linkage of Te$-_{eq}$O$_{ax}$–Te. It is stated that [9,15,16] a distorted TeO$_4$ tbp is the principal structural unit in tellurite glasses with high TeO$_2$-content. Increasing the content of modifier oxide leads to an increase in the fraction of TeO$_3$ trigonal pyramids. By using different techniques [17–19] it is deduced that with adding modifiers in tellurite glasses, there are regrouped tetrahedra besides to the tbp's in which the equatorial and axial sites of each tellurium atom has three and one oxygen atoms (TeO$_{3+1}$ units), respectively.

Tellurite glass-ceramics containing nanocrystals were obtained upon preparing oxyfluoride tellurite glass-ceramics [20–22]. Because of the easy devitrification of tellurite glasses, oxyfluoride tellurite glass-ceramics cannot attain a high degree of transparency. Several studies on the effects of replacing oxygen ions by fluorine ions were reported for oxyhalide tellurite glasses. In XZnF$_2$·(85 – X)TeO$_2$·12PbO·3Nb$_2$O$_5$ glasses (X = 0–40 mol%) [23] it has been found that addition of ZnF$_2$ allows substitution of a Te–F for Te–O bindings. Because F$^-$ ion has almost the same radius as O^{2-} ion, and its electronegativity is higher there is a high probability that oxygen ions will be replaced by fluorine ions. Interstitial positions could also be occupied by F$^-$ ions. In these glasses TeO$_3$, TeO$_{3+1}$ and/or Te(O,F)$_3$ and Te(O,F)$_{3+1}$ units are formed at the expense of TeO$_4$ units upon substituting ZnF$_2$ for TeO$_2$.

Fluorine ions also contribute to modification of borate glasses in a similar manner. Doweidar et al. [24–27] pointed out that F$^-$ ions mainly tend to modify the tetrahedral borate units in MF$_2$–B$_2$O$_3$ glasses (M = Ca, Ba, Cd and Pb). M$_{1/2}^{2+}$[BO$_{3/2}$F]$^-$ units can be formed in the borate network due to incorporation of MF$_2$. Formation of Na$^+$[BO$_{3/2}$F]$^-$ and Me$_{1/2}^{2+}$[BO$_{3/2}$F]$^-$ oxyfluoride structural units was proposed by Sokolov et al. [28] in MeF$_2$–Na$_2$B$_4$O$_7$ glasses where (Me = Mg, Ca, Sr and Ba). Recently, El Agammy et al. [29] proposed formation of Pb$_{1/2}^{2+}$[TeO$_{3+1}$]$^-$ and TeO$_{3/2}$F units in PbF$_2$–TeO$_2$ glasses and glass-ceramics through modifying TeO$_4$ tbp's units by F$^-$ ions.

The work reported here investigates the structure of NaF–TeO$_2$

---

* Corresponding author.
E-mail address: e.f.elagamy@gmail.com (E.F. El Agammy).

glasses and glass-ceramics, by using XRD, SEM, TEM, Raman and IR spectroscopy. Its main objective is to explore the type and concentration of structural units as a function of NaF content.

2. Experimental

As start materials with high purity (99%, Sigma-Aldrich), reagent grade of TeO_2 and NaF were used to prepare glasses and glass-ceramics with composition XNaF·(100–X)TeO_2 ($0 \leq X \leq 75$ mol%). After thorough mixing, the components were placed and melted in silica crucibles in an electric furnace, under normal atmospheric conditions. Batches were melted for 30 min, at 800–850 °C, depending on their respective compositions. The crucible was swirled repeatedly until the melt became visually homogeneous. Glass disks were obtained at room temperature after the melt was dropped on a steel plate and compressed by another one. Finally, a desiccator was used to keep the obtained samples until required.

X-ray diffractometer (Bruker AXS D8 Advance) was used to record X-ray diffraction patterns (XRD) of the prepared glass and glass-ceramic samples, using a Cu K_α X-ray tube radiation ($\lambda = 1.5406$ Å) with a Super Speed position sensitive detector and a Gobel Mirror. The range of the 2-theta scale was 4°–70° with 0.4 s as a dwell time.

A JEOL–JEM–2100 was used to carry out transmission electron microscopy (TEM) and obtain electron diffraction patterns (EDP), at an electron acceleration voltage of 200 kV. The microstructure and surface modification of the glass and glass-ceramic samples were investigated using a scanning electron microscope (SEM) model JEOL–JSM–6510 LV, with magnification up 40,000 X, operating at 20 kV and attached with an energy dispersive X-ray (EDX) spectrometer. Gold was used as a coating material for SEM and TEM investigations.

Raman spectra were recorded for powder samples with Bruker dispersive Raman microscope (Senterra model). The range of wavenumber is from 50 to 1200 cm^{-1}. The data were recorded at intervals of 4.4 cm^{-1} with two scans for each sample. A He/Ne laser at 532 nm and power of 10 mW was used to excite the specimen.

The infrared absorption spectra were obtained at room temperature in the range 400–2000 cm^{-1} by a Fourier transform infrared spectrometer (Mattson 5000 FTIR Spectrometer) with a resolution of 2 cm^{-1}. Transparent discs were made by subjecting portions of the mixture of 5 mg glass powder and 1 gm KBr to a load of 5 tons/cm^2. IR absorption spectra were recorded for freshly prepared discs. The deconvolution technique has been used to analyze the IR spectra [30,31].

3. Results and discussion

3.1. X-ray diffraction and electron microscopy

Fig. 1 represents the XRD patterns of fused NaF, fused TeO_2 and XNaF·(100–X)TeO_2 glasses and glass-ceramics ($10 \leq X \leq 75$ mol%). The pattern of fused NaF has two principal sharp peaks at $2\theta = 38.8°$ and $56.06°$, showing the crystalline nature of fused NaF. The pattern of fused TeO_2 exhibits many sharp peaks in the region ~22–66°. It is worth noting that, under normal conditions, tellurium oxide cannot form a glass without a modifier [11,12,32].

A broad diffraction hump in the range of 2θ from 12° to 44°, can be observed for glasses and glass-ceramics with NaF $\geq$10 mol%. This is characteristic of the presence of amorphous matrix in the glasses and glass-ceramics. A sharp decrease is shown in the intensity of the three major diffraction peaks at $2\theta = 26.09°$, 29.81° and 48.53° with the first addition of NaF (10 mol%). These peaks are related to α-TeO_2 crystalline phase (card 78-1713). The decrease in intensity of these peaks reflects a decrease in concentration of the TeO_4 tbp units. This might be accompanied by an increase in the concentration of TeO_3, TeO_{3+1} and/or $Te(O,F)_3$ and $Te(O,F)_{3+1}$ units. Similar structural changes have been observed in previous separate studies on lead and zinc fluorotellurite glasses [29,33]. In the composition range ($20 \leq X \leq 50$ mol%) new

diffraction peaks start appearing at ($2\theta = 27.62°$ and 29.35°), which belong to crystalline phases of $Te_2O_3F_2$ (card 89-0619).

For glasses with $20 \leq X \leq 30$ mol% the intensity of the peaks at $2\theta = 27.62°$ and 29.35°, increases with increasing NaF content, and then decreases for NaF $\geq$30 mol%. The decrease in intensity may be due to the decrease in quantity of TeO_2 available to form $Te_2O_3F_2$ crystal phase with increasing the NaF content.

For compositions with NaF > 50 mol%, the intensity of the diffraction peaks at $2\theta = 38.77°$ and 56.2° increases with increasing NaF content. These peaks belong to the NaF crystalline phase (cards 89-2956, 89-3614, 73-1922 and 36-1455) and are identical in position to those of fused NaF. The evolution of these peaks, with increasing intensity, suggests formation of crystalline NaF in these glasses and glass-ceramics. In crystalline NaF, Na$^+$ ions are octahedrally coordinated with F$^-$ ions [34]. By using Scherrer's equation in XRD patterns, we found that the mean size of this crystalline phase was ~20.50 nm at NaF = 65 mol%. Therefore, for higher NaF content (> 50 mol%) it is assumed that most of NaF forms a crystalline phase from NaF$_6$ octahedral units. Recently, El Agammy et al. [29] stated that in xPbF$_2$·(100-x)TeO_2 glasses and glass-ceramics ($0 \leq x \leq 90$ mol%), for PbF$_2$ > 50 mol%, amorphous and crystalline polyhedral units were formed, where PbF$_2$ forms cubic crystals. Also, Rojo et al. [35] indicated that, in XLiF·(100-X)TeO_2 glasses with LiF > 50 mol%, characteristic peaks of crystalline LiF were observed in the X-ray diffraction patterns.

Electron diffraction patterns in certain regions of the TEM micrographs show amorphous and crystalline phases (Fig. 2). Crystalline phases can be correlated with the XRD patterns in Fig. 1. In the composition range ($20 \leq X \leq 50$ mol%) the peaks shown in Fig. 1 are related to crystalline $Te_2O_3F_2$ phase. This phase appears at NaF = 30 mol% in transmission electron micrographs as dark regions spreading within the structure as in Fig. 2a.

The diffused circles in EDP patterns in Fig. 2a are characteristic of the amorphous matrix at NaF = 30 mol%, which might be characteristic of a NaF–TeO_2 phase. Fig. 2b shows that for a higher concentration of NaF (65 mol%) there is a crystalline phase. By comparing with Fig. 1, this phase might be NaF. It appears as dark regions in the TEM micrograph. The amorphous regions identified by EDP in Fig. 2b appear in TEM micrograph as gray particles. These particles are assumed to contain a large portion of the glassy NaF phase.

The morphology of the NaF–TeO_2 glasses and glass-ceramics was investigated using SEM. Before using SEM, some samples were etched in 5% HF solution for 10 min. Fig. 3 describes the microstructure of the glasses and glass-ceramics samples with NaF = 0, 10, 30, 50 and 65 mol% after etching process.

Fig. 3a shows the SEM micrograph of fused TeO_2 (NaF = 0 mol%). The general feature is the presence of discrete particles of different sizes, dispersed in a continuous matrix. On the basis of XRD pattern Fig. 1, these particles can be attributed to α-TeO_2, the dominant crystalline phase for this composition. The base matrix in Fig. 3a may be formed of residual disordered TeO_2 phase that could not crystallize. Fig. 3b (NaF = 10 mol%) shows the presence of small white grains dispersed on the surface and in the bulk of mostly rectangular rods of width ~ 50–70 μm. At higher magnification, it appears that the white grains form agglomerates dispersed in a continuous matrix (the darker background base). By comparing with the related XRD pattern in Fig. 1, the dominant crystalline phase in this composition must be α-TeO_2. Therefore, the grain-like aspect seen on the SEM micrographs is likely due to the presence of α-TeO_2 phase, with a background base of glassy NaF–TeO_2 matrix. Fig. 1 shows that the XRD pattern of sample with NaF = 10 mol% has the broadest hump in all samples which reveals that this sample contains the greatest fraction of the glassy phase through the system.

Condensed agglomerates are seen on the micrograph of the sample containing 30 mol% NaF (Fig. 3c); they are different in shape from those in Fig. 3b. These agglomerates consist of clusters of different sizes.
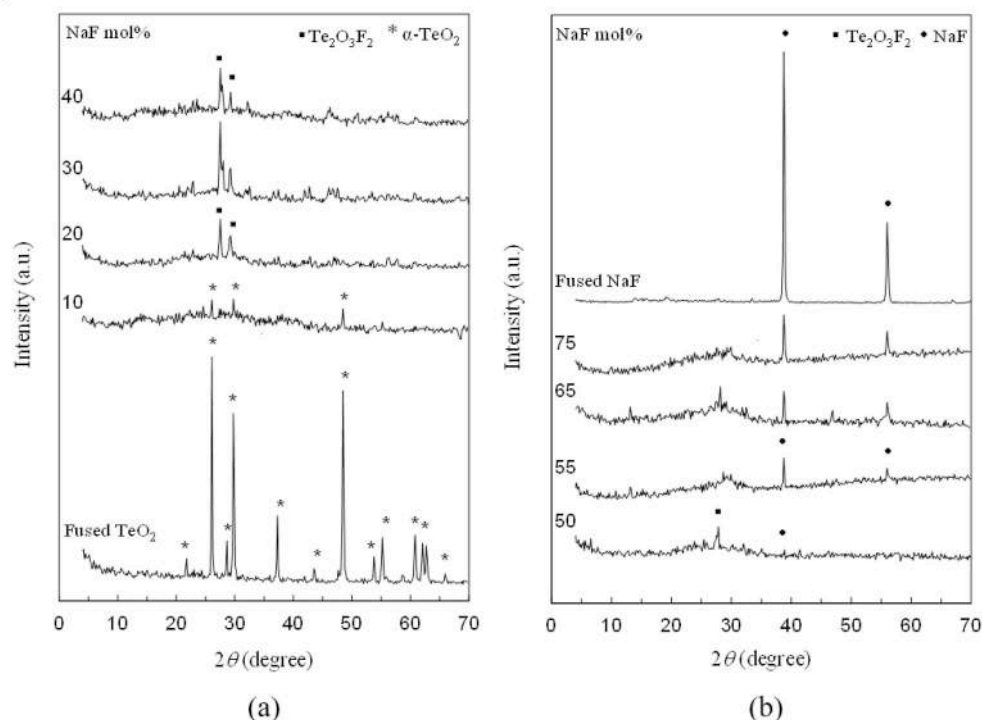
Fig. 1. XRD patterns of fused TeO_2, fused NaF and XNaF·(100–X)TeO_2 glasses and glass-ceramics where ($0 \leq X \leq 75$ mol%) divided to two figures (a) ($0 \leq X \leq 40$ mol%), (b) ($50 \leq X \leq 75$ mol%) and fused NaF.

As the XRD pattern in Fig. 1 indicates, the prevalent crystalline phase in this composition is $Te_2O_3F_2$.

The micrograph of the sample with 50 mol% NaF (Fig. 3d) shows the presence of two types of precipitates: micro-rods and platelets. Based on the XRD patterns (Fig. 1), the crystalline phases found in this composition are NaF and $Te_2O_3F_2$. By comparing Fig. 3d with Fig. 3c, it can be assumed that the micro-rods in Fig. 3d are developed from the agglomerates appearing in Fig. 3c, i.e. these rods form the $Te_2O_3F_2$ crystalline phase. It follows that the platelets in Fig. 3d are the basis of crystalline NaF phase. According to Fig. 1, the XRD patterns of samples with NaF > 50 mol% are dominated by peaks of crystalline NaF. Therefore, it is supposed that in sample with X = 65 mol%, NaF is present in the glass-ceramic matrix in the form of amorphous and crystalline phases, as observed by SEM (Fig. 3e). Fig. 3e shows white agglomerates, assumed to be crystalline NaF developed from the platelets in Fig. 3d, in the structure of glass-ceramic. These agglomerates are discrete and spread out within the structure. It is expected that the fraction and degree of crystallinity increase with increasing NaF content. XRD patterns in Fig. 1 show that when the content of NaF in the samples with NaF > 50 mol% increases, the intensity of the peaks related to crystalline NaF increases. Fig. 4a shows higher magnification of the agglomerates of crystalline NaF phase in the sample containing 65 mol% NaF without etching, whereas the agglomerates have spherical form. They are discrete, separated and can be observed in samples with and without etching. The appearance of these agglomerates in samples, before (Fig. 4a) and after (Fig. 3e) etching, reveals that the etching process is useful to get more clarification of the formed phases without other influence on the structure. By using ImageJ software program in SEM micrographs of the sample 65 mol% NaF (Fig. 3e) it is found that the mean size of particles formed in this sample is ~ (21.52 ± 12) nm. The distribution of the particle size has a maximum in the region from 10 to 20 nm and represents ~50% of the total distribution as shown in Fig. 4b. EDX results for different regions of the sample with 65 mol% NaF (Fig. 5), as an example, reveal that only Na, F, Te and O elements are observed. This indicates that the sample has no contamination from the crucible.

3.2. Raman spectra

Raman [14] and NMR [36] spectroscopies revealed the formation of a three-dimensional network of paratellurite α-TeO_2. The basic building unit is TeO_4 tbp, sharing vertices and having just only Te–$_{eq}O_{ax}$–Te linkages. Further, pure TeO_2 glass is built up of distorted TeO_4 tbp units. It has been confirmed by many reports [37,38] on Raman scattering spectra that increasing the content of alkali- and/or alkaline-earth oxides generates a gradual change of the structural unit of TeO_2-based glasses, from an asymmetric TeO_4 tbp to a TeO_3 trigonal pyramid (tp) through TeO_{3+1} polyhedra. Tatar et al. [39] showed that, for a binary CdF_2–TeO_2 glass system, with compositions below 20 mol% CdF_2, the transformation rate of TeO_4 to TeO_{3+1} units is constant, and that it decreases for CdF_2 > 20 mol%. For compositions with CdF_2 > 15 mol% there is an increase of the transformation from TeO_4 to TeO_3 units. Some authors [40,41] showed that, in oxyfluoride tellurite glasses, the strong Te–O covalent network tends to be broken up by F$^-$ ions by forming non-bridging, ionic M–F bonds (where M is a cation).

The spectra shown in Fig. 6 can be used to get the fraction N_4 of four coordinated tellurium atoms TeO_4 tbp in the studied glasses and glass-ceramics. N_4 is the ratio of the concentration of tellurium atoms in trigonal bipyramid units with four bridging oxygen atoms to the total concentration of tellurium atoms in the matrix. By using the deconvolution technique [31,42,43], the area under the absorption envelopes can be determined and used to calculate N_4 in Raman spectra (Appendix 1). This technique was recently used for tellurite glasses by El Agammy et al. [29] for Raman and IR spectroscopies. Fig. 7 clarifies the deconvolution, in Gaussian bands, of IR spectrum for the sample 50NaF–50TeO_2, as an example.

Table 1 shows the assignment used in the deconvolution technique for Raman and IR spectra. Fig. 8 shows the dependence of N_4 as obtained from Raman and IR spectra on NaF content. The average N_4 and theoretical values calculated from the formula $N_4 = 1-2X/(100-X)$, where X is the concentration of NaF (mol%) [29,36] in XNaF·(100–X)TeO_2 glasses and glass-ceramics, are also presented. It appears
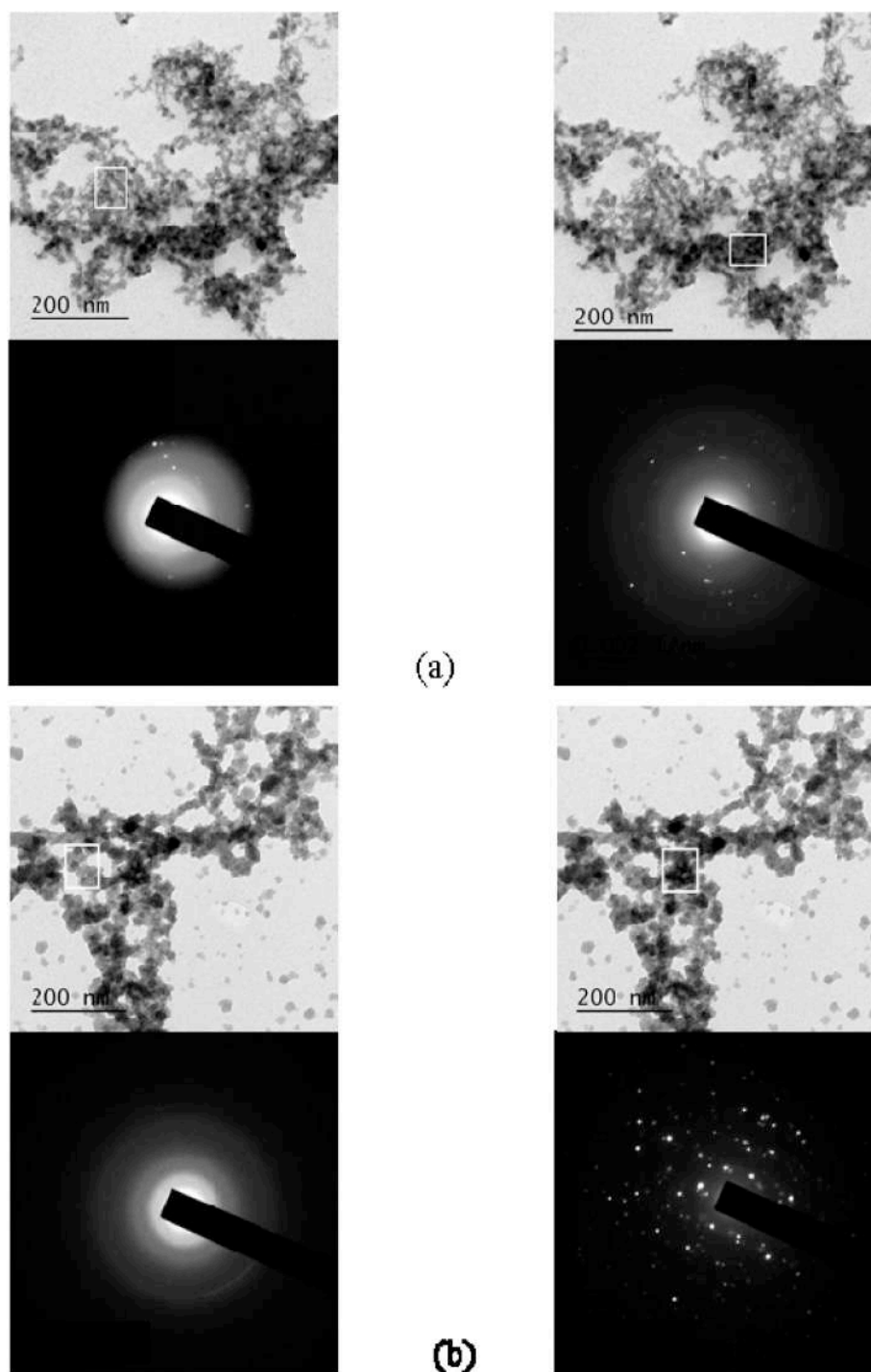
Fig. 2. Transmission electron micrographs and electron diffraction patterns of NaF–TeO$_2$ glasses and glass-ceramics having (a) 30 and (b) 65 mol% NaF. Electron diffraction patterns are obtained from the area inside the showed rectangles.

that N_4 decreases when increasing the content of NaF. The curve can be divided in two regions: the first one is that for NaF $\leq$10 mol%, where N_4 decreases almost linearly with increasing NaF content, and the second one is the region for NaF > 10 mol%, where N_4 tends to reach a steady value ($\sim$0.60 $\pm$ 0.05). A similar behavior [29] was observed in xPbF$_2\cdot$(1-x)TeO$_2$ glasses and glass-ceramics (0 $\leq$ x $\leq$ 90 mol%) where N_4 decreased almost linearly for PbF$_2$ $\leq$ 10 mol% and for PbF$_2$ > 10 mol%, it decreases gradually with a decreasing rate. Further, the change was rather limited for PbF$_2$ $\geq$ 30 mol%.

Fig. 9 presents a graphical illustration of different structural units in NaF–TeO$_2$ glasses and glass-ceramics. These are proposed forms of the

evolved structural units when NaF is added to TeO$_2$. Upon introducing NaF, the bond between O and Te atoms in Te-$_{eq}$O$_{ax}$-Te linkage will be broken and [TeO$_{3+1}$]$^-$ with one non-bridging oxygen and TeO$_{3/2}$F units are formed (Fig. 9b). The negative charge on [TeO$_{3+1}$]$^-$ unit will be compensated with the positive charge of Na$^+$ ion and form a Na$^+$[TeO$_{3+1}$]$^-$ unit. For NaF > 10 mol% two TeO$_{3/2}$F units are linked together to form a Te$_2$O$_3$F$_2$ unit with three bridging oxygens (Fig. 9c), then crystalline octahedral NaF phase is formed. To understand the behavior in Fig. 9, it is worth recalling the theoretical hypothesis introduced by Sakida et al. [36]. In the composition xNaF·(1-x)TeO$_2$, with x being the molar fraction of NaF, the molar fraction of tellurium is
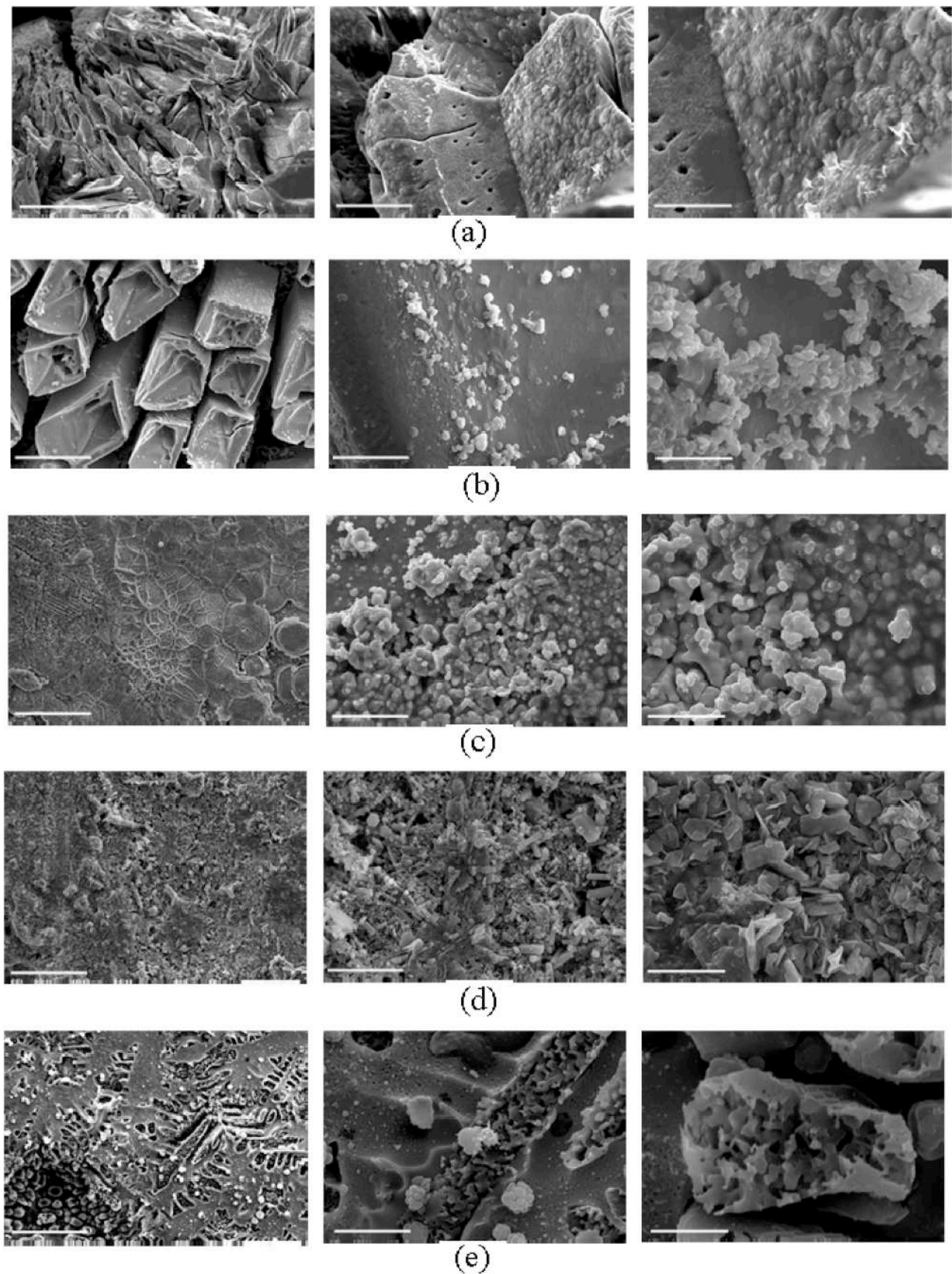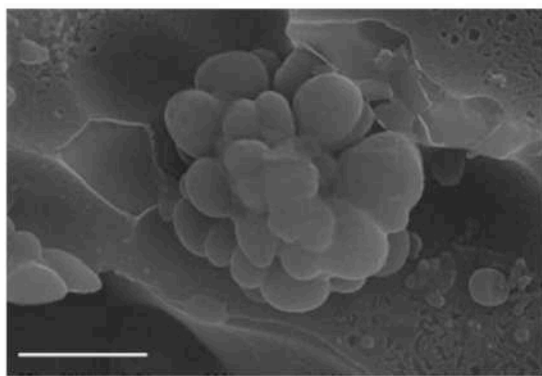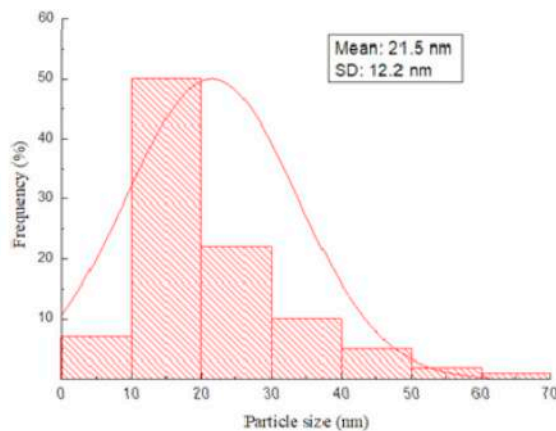
Fig. 3. Scanning electron micrographs of NaF–TeO$_2$ glasses and glass-ceramics having (a) 0, (b) 10, (c) 30, (d) 50 and (e) 65 mol% NaF after etching. From left, figures have three magnifications x500, x2500 and x5000 for each sample with length of scale bar 50 μm, 10 μm and 5 μm, respectively.

Fig. 4. (a) Scanning electron micrograph before etching of 65NaF–35TeO$_2$ glass-ceramic at x10000 magnification and 1 μm length of scale bar, (b) distribution of particle size.
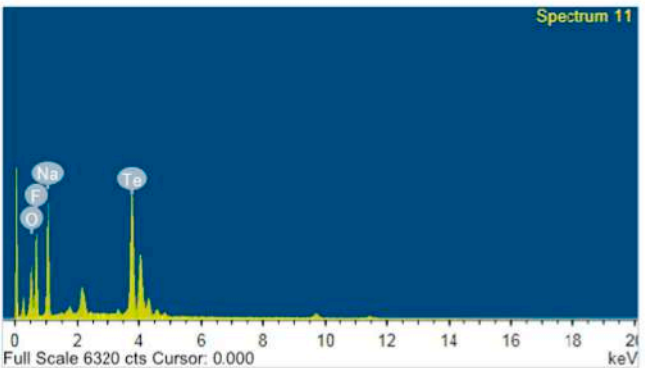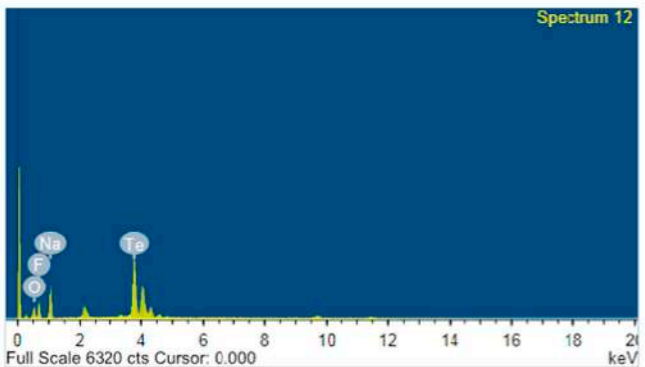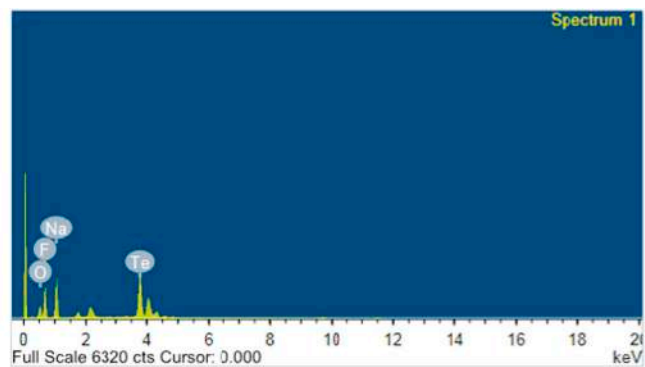

Fig. 5. Energy dispersive X-rays (EDX) analysis for different regions of the sample with 65 mol% NaF.
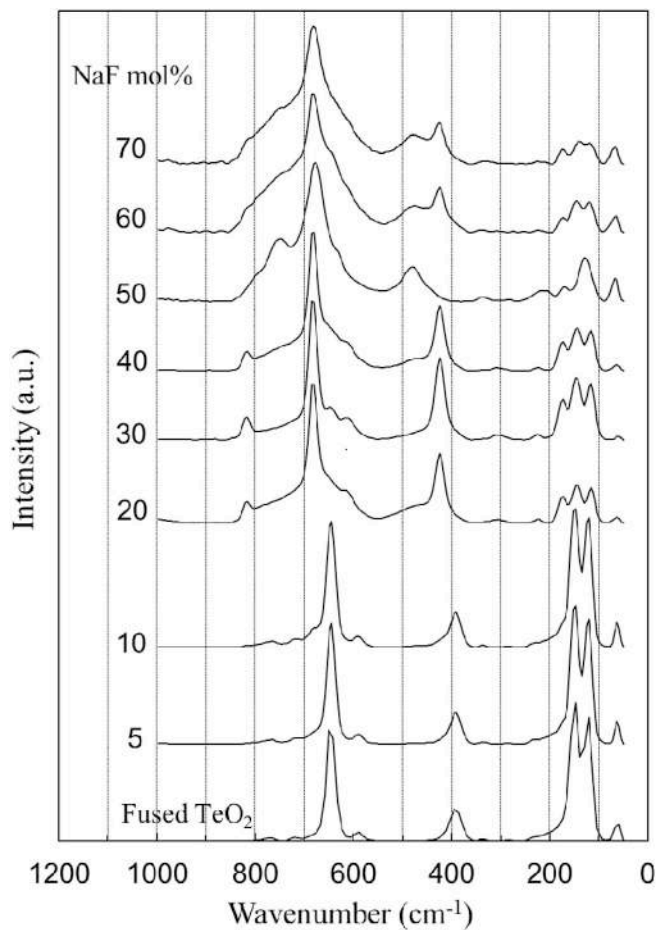
Fig. 6. Normalized Raman spectra of the XNaF·(100–X)TeO$_2$ TeO$_2$glasses and glass-ceramics. Numbers on the graphs refers to the content of NaF (mol%).

(1–x), and every NaF molecule converts two TeO$_4$ to [TeO$_{3+1}$]$^-$ and TeO$_{3/2}$F units. The number of modified units is 2x, hence N_3 and N_4 are represented by:

$$N_3 = 2x/(1 – x) \tag{1}$$

$$N_4 = 1 – N_3 \tag{2}$$

where N_3 is the ratio of concentration of all tellurium atoms that do not

Fig. 7. Deconvolution of Raman spectrum of the glass-ceramic 50NaF–50TeO$_2$ as an example.

have four bridging oxygens to the total concentration of tellurium atoms in the matrix. The data presented in Fig. 8 can be analyzed 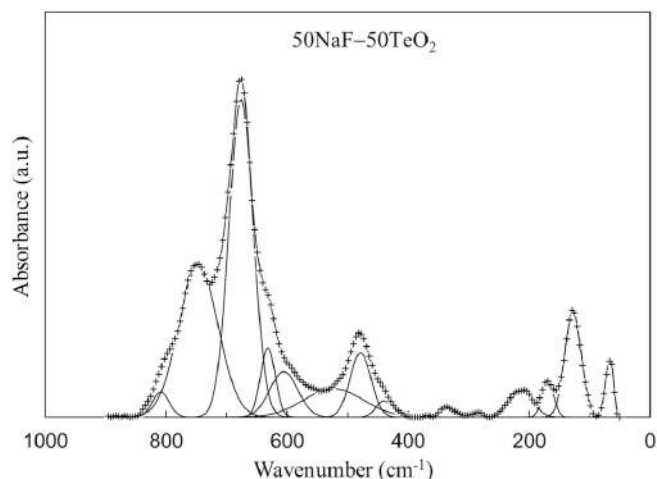following the same method as the one used in previous studies [26,27,29]. The almost linear decrease of N_4 with NaF content up to 10 mol% implies that in the glass network the entire content of NaF converts TeO$_4$ units into [TeO$_{3+1}$]$^-$ and TeO$_{3/2}$F units. In this case, each NaF molecule converts two TeO$_4$ units into TeO$_{3/2}$F and Na$^+$[TeO$_{3+1}$]$^-$ units. In addition to these units, NaF partially modifies the tellurite network in the region of NaF > 10 mol% forming Te$_2$O$_3$F$_2$ crystal phase and the rest of NaF starts to form its own amorphous matrix in the form of NaF$_6$ octahedra. This conclusion is consistent with the crystalline phases exhibited in the XRD patterns of samples with NaF > 10 mol% (Fig. 1).

In TeF$_4$ crystal, the Te–F stretching vibration absorption peaks in Raman spectra occur at 190, 293, 337, 395, 567, 659, 696 and 731 cm^{-1} [59]. Yoko et al. [60] stated that, according to the Bent rule, F atoms added to TeO$_2$ in LiF–TeO$_2$ glasses possibly take an axial position where the electronegativity of F atom is larger than that of O atom. It is suggested that, when adding NaF to TeO$_2$ it breaks Te–$_{eq}$O$_{ax}$–Te bridging bond. F will take an axial position and the formed non-bridging oxygen in an equatorial position will have high ability of donating electrons [60]. This causes strengthening of the Te–O$_{eq}$ bond and the negative charge on this bond will be compensated with that of Na$^+$ ion.

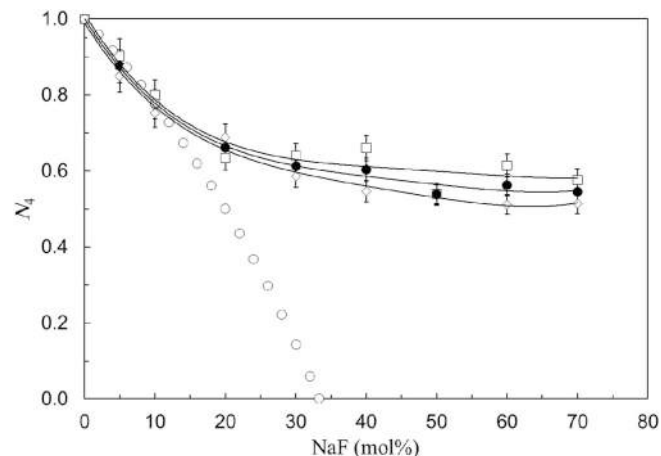Based on the above assumptions, the concentration of developed

Fig. 8. Compositional change of the fraction N_4 of TeO$_4$ tbp in the glasses and glass-ceramics investigated. N_4 values are calculated from Raman spectra (□), IR spectra (◊), average values obtained from Raman and IR spectra (●) and theoretical data (○). N_4 values are accurate to ± 7%.
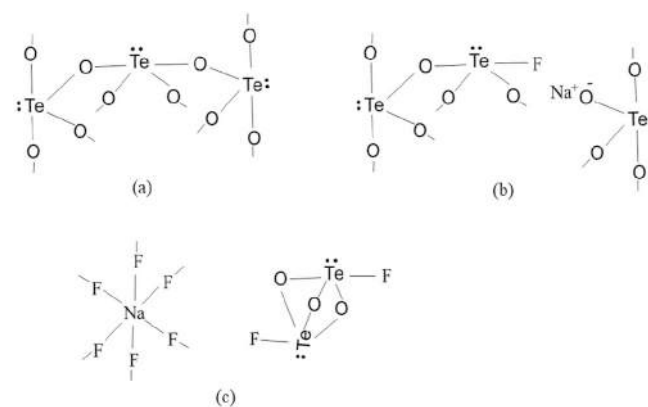

Fig. 9. Schematic presentation of different structural units in NaF–TeO$_2$ glasses and glass-ceramics. (a) α-TeO$_2$ (TeO$_4$ units) (b) TeO$_{3/2}$F and Na$^+$[TeO$_{3+1}$]$^-$ units (c) Te$_2$O$_3$F$_2$ and NaF$_6$ units.

structural units can be obtained as follows:

$$C_{Te4} = N_4 \, C_{Te} \tag{3}$$

$$C_{Te3} = C_{Te} - N_4 \, C_{Te} \tag{4}$$

Table (1)
Band assignment of IR and Raman spectra for XNaF·(100–X)TeO$_2$ glasses and glass-ceramics.

| Infrared bands		Raman bands	
Band center (cm^{-1})	Assignment	Band center (cm^{-1})	Assignment
418–446	Cationic vibration [44–46]	63, 122, 149, 159, 392, 588, 646, 649	Te–O stretching vibrations in TeO$_4$ [14], [from Raman spectrum of fused TeO$_2$ in present study]
~565	Te–O vibrations, where the O anions were considered as NBO [47]	~270	bending vibration of TeO$_3$ tp having two or three NBO atoms [48]
590–600	Te–O stretching vibrations in TeO$_{3+1}$ units [49,50]	~330	bending vibration of TeO$_3$ tp having two or three NBO atoms [51]
620–670	Te–O stretching vibrations in TeO$_4$ [49]	430–460	Bending and stretching vibrations of Te–O–Te or O–Te–O linkages [14,37,52–54]
677–688	Te–O stretching vibrations in TeO$_4$ [46]	600–615	Te–O stretching vibrations in TeO$_4$ [14,37,55]
680–724	Te–O bending vibrations in TeO$_3$ units and TeO$_6$ units [44]	660–690	Te–O stretching vibrations in TeO$_4$ [38,56–58]
756–767	Te–O bending vibrations in TeO$_3$ [46]	720–760	Te–O bending vibrations in TeO$_3$ units [37,55,58]
770–790	Te–O stretching vibrations in TeO$_4$ [49]	770–780	Te–O bending vibrations in TeO$_3$ units [37,55]
817–875	Stretching vibrations mode of TeO$_3$ tp with NBOs [47]	767 and 293	Te(O, F)$_3$ units [58]
		677 and 443	Te(O, F)$_4$ units [58]
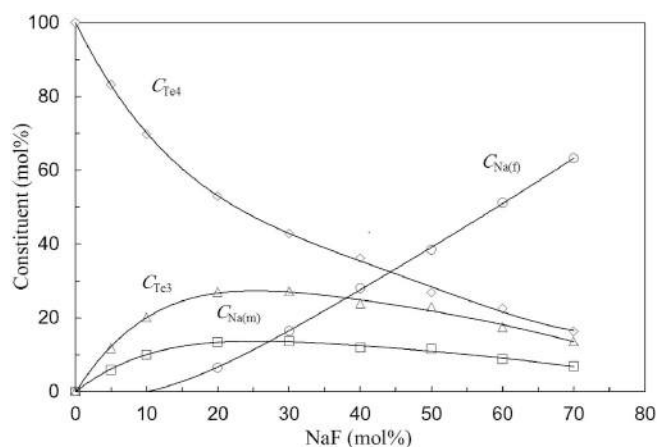
Fig. 10. Dependence on NaF content of C_{Te4}, C_{Te3}, $C_{Na(m)}$ and $C_{Na(f)}$. C_{Te3} is the quantity of TeO_2 (mol%) converted to TeO_3, TeO_{3+1} and/or $Te(O,F)_3$, $Te(O,F)_{3+1}$ units, C_{Te4} represents the quantity of TeO_2 that forms TeO_4 tbp units. $C_{Na(m)}$ attributes to the quantity of NaF that works as modifier and $C_{Na(f)}$ is that creating NaF_6 units (the NaF former part).

$$C_{Na(m)} = C_{Te3}/2 \tag{5}$$

$$C_{Na(f)} = C_{Na} - C_{Na(m)}. \tag{6}$$

Here C_{Te3} is the quantity (mol%) of TeO_2 converted to TeO_3, TeO_{3+1} and/or $Te(O,F)_3$, $Te(O,F)_{3+1}$ units, C_{Te} is the total TeO_2 content in glass and glass-ceramic. C_{Te4} represents the quantity of TeO_2 in the form of TeO_4 tbp units. $C_{Na(m)}$ refers to the quantity of NaF in (mol%) that works as modifier and $C_{Na(f)}$ is the NaF former part, which forms NaF_6 units. The quantities in Eqs. (3)–(6) can be obtained by using the average N_4 values obtained from the Raman and IR spectra (Fig. 8). Fig. 10 shows that, with increasing NaF content, C_{Te4} decreases almost linearly in two regions. These are $0 \leq NaF \leq 10$ mol% and $20 \leq NaF \leq 70$ mol%, where the rate of change is lower in the second region. At the same time, C_{Te3} and $C_{Na(m)}$ show a maximum at 20 mol% NaF. $C_{Na(f)}$ seems to be negligible up to 10 mol% NaF and then it steadily increases with increasing NaF content. Decreasing of C_{Te4} and increasing of C_{Te3} for NaF ≤ 20 mol% reflect greater ability of NaF to modify the tellurite matrix in this region, as deduced from the high decreasing rate in N_4 (Fig. 8). The increase of $C_{Na(f)}$ for NaF > 10 mol% and the decrease of C_{Te3} and $C_{Na(m)}$ for NaF ≥ 20 mol% indicate that NaF starts to form its own matrix, beside modifying the tellurite network. There is a limited decrease in N_4 for NaF ≥ 20 mol% (Fig. 8), which might indicate that most of the added NaF content is consumed for forming its matrix and sharing in forming $Te_2O_3F_2$ phase. A similar trend was noticed before in PbF_2–TeO_2 glasses and glass-ceramics [29]. The conclusions drawn from this analysis are in good agreement with those obtained from the XRD, TEM and SEM results.

3.3. Infrared spectra

The IR spectrum of pure TeO_2 glass is dominated by a shoulder at $\sim$780 cm^{-1} and a major wide absorption band at $\sim$635 cm^{-1} [50]. According to some investigators [49], the first band is related to vibrations of the symmetric Te–O_{ax} bond and the second one is related to asymmetric vibrations of the Te–O_{eq} bond in the units of TeO_4. In a recent study based on first principles calculations [61], the bond order has values of 0.3 and 1.7 for these two bonds, respectively. So, the first bond (2.12 Å) can be categorized as mostly covalent, while the second bond (1.87 Å) is most likely of electrostatic nature.

Yoko et al. [60] showed that the center of axial band observed at ~ 628 cm^{-1} in the infrared spectra of LiX–TeO_2 glasses (X = Br, Cl, F and O) shifted towards lower wavenumbers with increasing LiX content. The extent of the shift in the band center followed the sequence:
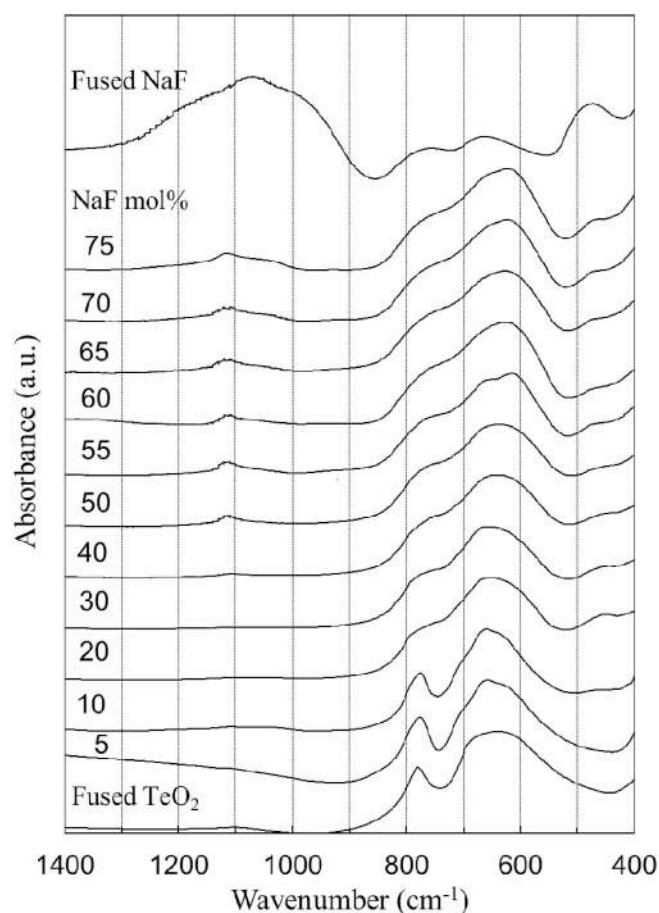
Fig. 11. Normalized IR spectra of fused TeO_2, XNaF·(100–X)TeO_2 glasses and glass-ceramics and fused NaF. Numbers on the graphs refer to the content of NaF (mol%).

Br < Cl < F < O. A decrease in the bond strength of Te–O_{ax} in the same order revealed that the weakening of a bond is responsible for the shift towards lower wavenumbers.

The spectra shown in Fig. 11 can be used to obtain the N_4 fraction of four coordinated tellurium atoms TeO_4 tbp in the studied glasses and glass-ceramics. By using the deconvolution technique we can calculate N_4 from IR spectra. Fig. 12 clarifies an example of the deconvolution parameters and the deconvoluted pattern of the IR spectra of XNaF·(100–X)TeO_2 glasses and glass-ceramics. Deconvolution data are given in Appendix 2. Fig. 8 shows the dependence of N_4 which is calculated

Fig. 12. Deconvolution of the IR spectrum of the 50NaF–50TeO$_2$ sample.

from Raman and IR spectra. There is a similarity in behavior between the curve of N_4 related to Raman spectra and that of IR spectra and the values of N_4 are close to each other with an average standard deviation ($\pm$ 0.038). Similar conclusions to those obtained from the analyzed Raman spectra can be drawn for the structural changes of TeO_2 with increasing NaF content.
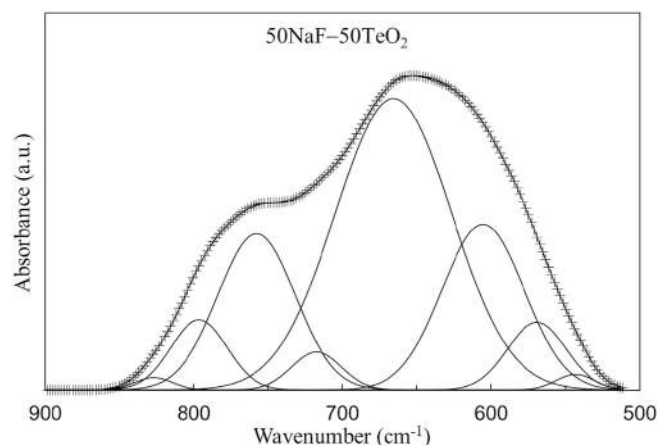
4. Conclusion

NaF enters the glass and glass-ceramic network to convert TeO_4 units into TeO_3, TeO_{3+1} and/or $Te(O,F)_3$, $Te(O,F)_{3+1}$ with a non-bridging Te–F bond. The remaining NaF enters the structure in both amorphous and crystalline phase forms, presumably as NaF_6 octahedra. It also participates in the formation of the crystalline $Te_2O_3F_2$ phase in compositions with NaF > 10 mol% as evidenced by XRD. Raman and FTIR spectroscopies are used to obtain the fraction N_4 of TeO_4 tbp units. The latter could be used to calculate the concentration of the various structural species in the studied compositions. Separated agglomerates of $Te_2O_3F_2$ phase forming grains of different size are detected by SEM. For NaF > 50 mol%, crystalline NaF is the dominant phase.

Declaration of competing interest

The authors declare that they have no known competing financial interests or personal relationships that could have appeared to influence the work reported in this paper.

Appendices

Appendix (1)

Deconvolution parameters of Raman spectra of the XNaF·(100–X)TeO$_2$ glasses and glass-ceramics. *B.C* is the component band centre (cm^{-1}), *A* is the area of the component bands and *R.A.* is the relative area (%) of the component band.

NaF (mol%)	Structural units and band parameters															
0	group	TeO_4														
	B.C	62.5	121.6	148.7	158.9	392.1	588.4	645.7	649.4	718.1	772.4					
	A	1.9	15.7	17.5	12.1	7.0	1.2	15.2	6.5	0.6	0.7					
	R.A.	2.4	20.0	22.3	15.4	8.9	1.6	19.4	8.3	0.7	0.8					
5	*group*	TeO_4				TeO_3	TeO_4				TeO_3					
	B.C	62.7	121.3	148.6	151.2	220.1	392.4	589.8	640.8	645.8	675.7	718.9	770.8			
	A	2.1	14.9	15.5	14.7	1.6	7.3	1.9	6.6	13.2	4.2	0.9	1.5			
	R.A.	2.5	17.7	18.3	17.4	1.9	8.6	2.2	7.9	15.6	5.0	1.1	1.8			
10	*group*	TeO_4				TeO_3	TeO_4	TeO_3	TeO_4	TeO_3	TeO_4	TeO_3				
	B.C	62.8	121.4	148.6	153.2	222.1	390.7	407.9	590.1	629.5	646.0	675.7	718.7	769.5		
	A	2.3	16.4	16.4	14.7	1.2	5.2	3.8	2.1	3.3	17.9	6.2	1.3	2.4		
	R.A.	2.5	17.6	17.6	15.7	1.3	5.6	4.1	2.2	3.6	19.2	6.6	1.4	2.6		
20	*group*	TeO_4				TeO_3				TeO_4				TeO_3		
	B.C	64.5	115.5	142.6	158.9	175.5	224.3	423.5	456.7	590.0	610.2	671.1	682.0	771.1	817.8	
	A	0.7	5.1	5.2	3.0	2.7	0.5	8.8	16.2	1.5	1.7	40.3	13.0	10.5	1.9	
	R.A.	0.6	4.6	4.7	2.7	2.5	0.4	8.0	14.6	1.3	1.5	36.3	11.7	9.4	1.7	
30	*group*	TeO_4			TeO_3					TeO_4				TeO_3		
	B.C	60.7	116.2	145.3	174.6	221.1	303.7	423.4	431.9	608.6	645.1	675.8	682.1	789.5	818.2	
	A	0.4	9.0	11.4	6.6	1.2	1.4	11.1	10.1	1.9	1.1	26.5	17.2	3.8	2.4	
	R.A.	0.4	8.7	10.9	6.3	1.2	1.3	10.7	9.7	1.8	1.1	25.5	16.5	3.7	2.3	
40	*group*	TeO_4			TeO_3					TeO_4				TeO_3		
	B.C	64.4	115.8	144.2	174.3	223.2	303.9	423.5	450.5	609.1	668.3	672.5	682.2	768.5	817.9	
	A	0.8	6.2	8.2	4.5	0.6	0.7	8.7	11.1	1.1	37.2	4.7	13.0	8.5	1.8	
	R.A.	0.7	5.8	7.6	4.2	0.6	0.7	8.1	10.4	1.0	34.8	4.4	12.2	7.9	1.7	
50	*group*	TeO_4			TeO_3					TeO_4			TeO_3			
	B.C	67.2	127.7	168.9	214.1	334.6	440.3	478.8	523.4	605.7	631.9	676.2	746.8	809.1		
	A	2.8	10.6	2.4	3.9	0.9	1.6	8.2	10.4	7.8	6.2	47.0	36.5	2.6		
	R.A.	2.0	7.5	1.7	2.8	0.7	1.1	5.8	7.4	5.5	4.4	33.3	25.9	1.8		
60	*group*	TeO_4			TeO_3								TeO_4			TeO_3
	B.C	67.5	118.2	145.6	174.7	222.8	326.0	424.1	424.3	481.1	522.9	568.8	604.9	669.3	681.8	763.0	813.0
	A	2.3	5.0	5.9	2.0	0.3	0.6	3.0	9.7	11.0	0.6	3.9	0.6	74.3	7.9	26.2	3.1
	R.A.	1.4	3.2	3.8	1.2	0.2	0.4	1.9	6.2	7.0	0.4	2.5	0.4	47.5	5.1	16.8	2.0
70	*group*	TeO_4			TeO_3								TeO_4			TeO_3
	B.C	68.1	115.1	140.4	173.8	221.2	327.7	424.2	430.2	478.6	506.2	571.1	610.2	675.3	681.2	758.5	813.9
	A	2.4	3.1	4.8	2.1	0.6	0.8	2.8	9.2	4.6	10.7	2.0	9.5	58.6	8.8	27.4	3.8
	R.A.	1.6	2.0	3.2	1.4	0.4	0.5	1.9	6.1	3.0	7.1	1.3	6.3	38.8	5.8	18.1	2.5

Appendix (2)

Deconvolution parameters of the infrared spectra of the XNaF·(100–X)TeO$_2$ glasses and glass-ceramics. *B.C* is the component band centre (cm^{-1}), *A* is the area of the component bands and *R.A.* is the relative area (%) of the component band.

NaF (mol%)	Structural units and band parameters								
0	group	TeO_4							
	B.C	521	625	684	694	748	781	784	
	A	10.6	129.0	23.3	2.9	0.8	10.3	33.4	
	R.A.	5.0	61.4	11.1	1.4	0.4	4.9	15.9	
5	group	TeO_3		TeO_4	TeO_3	TeO_4		TeO_3	TeO_3
	B.C	487	539	637	669	707	770	783	833
	A	1.1	10.5	120.8	6.9	10.7	3.1	29.0	5.6
	R.A.	0.6	5.6	64.3	3.7	5.7	1.6	15.4	3.0
10	group	TeO_3	TeO_4		TeO_3	TeO_4		TeO_3	
	B.C	571	641	667	703	773	781	830	
	A	9.7	84.9	3.6	26.7	0.8	26.2	1.6	
	R.A.	6.3	55.3	2.3	17.4	0.5	17.0	1.1	
20	group	TeO_3	TeO_4		TeO_3	TeO_3	TeO_4		TeO_3
	B.C	576	612	637	668	714	757	795	824
	A	13.5	30.9	0.7	79.9	5.7	32.4	7.1	1.9
	R.A.	7.8	18.0	0.4	46.4	3.3	18.8	4.1	1.1
30	group	TeO_3			TeO_4	TeO_3		TeO_4	TeO_3
	B.C	538	571	609	671	716	754	791	826
	A	0.5	9.0	34.8	88.0	2.7	23.3	14.8	2.4
	R.A.	0.3	5.1	19.9	50.2	1.5	13.3	8.4	1.4
40	group	TeO_3			TeO_4	TeO_3		TeO_4	TeO_3
	B.C	541	569	606	666	716	757	796	826
	A	0.9	9.3	36.2	90.4	4.2	30.9	9.6	1.3
	R.A.	0.5	5.1	19.8	49.4	2.3	16.9	5.2	0.7
50	group	TeO_3			TeO_4	TeO_3		TeO_4	TeO_3
	B.C	543	569	605	666	717	758	797	827
	A	1.6	10.7	36.6	91.1	5.1	32.6	10.6	1.2
	R.A.	0.9	5.6	19.3	48.1	2.7	17.2	5.6	0.7
60	group	TeO_3			TeO_4	TeO_3	TeO_4	TeO_3	
	B.C	552	574	608	664	741	780	809	
	A	2.9	11.7	39.8	83.3	32.8	13.6	5.2	
	R.A.	1.6	6.2	21.0	44.0	17.3	7.2	2.7	
70	group	TeO_3			TeO_4	TeO_3	TeO_4	TeO_3	
	B.C	551	572	604	655	727	774	807	
	A	2.0	8.4	35.8	76.1	37.2	18.7	6.4	
	R.A.	1.1	4.5	19.4	41.2	20.2	10.1	3.5	

References

[1] Z.A.S. Mahraz, M.R. Sahar, S.K. Ghoshal, M.R. Dousti, Concentration dependent luminescence quenching of Er^{3+} doped zinc boro-tellurite glass, J. Lumin. 144 (2013) 139–145.

[2] N. Elkhoshkhany, S.Y. Marzouk, S. Shahin, Synthesis and optical properties of new fluoro-tellurite glass within (TeO_2-ZnO-LiF-Nb_2O_5-NaF) system, J. Non-Cryst. Solids 472 (2017) 39–45.

[3] S. Sakida, S. Hayakawa, T. Yoko, Part 2.^{125}Te NMR study of M_2O-TeO_2 (M = Li, Na, K, Rb and Cs) glasses, J. Non-Cryst. Solids 243 (1999) 13–25.

[4] M.P. Smayev, V.V. Dorofeev, A.N. Moiseev, A.G. Okhrimchuk, Femtosecond laser writing of a depressed cladding single mode channel waveguide in high-purity tellurite glass, J. Non-Cryst. Solids 480 (2018) 100–106.

[5] Z. Hou, Z. Xue, S. Wang, Synthesis and spectroscopic properties of Er^{3+} doped CaF_2 nanocrystals in transparent oxyfluoride tellurite glass-ceramics, J. Alloys Compd. 514 (2012) 109–112.

[6] N. Jaba, H.B. Mansour, B. Champagnon, The origin of spectral broadening of 1.53 μm emission in Er^{3+} doped zinc tellurite glass, Opt. Mater. (Amst) 31 (2009) 1242–1247.

[7] G. Upender, C.P. Vardhani, S. Suresh, A.M. Awasthi, V.C. Mouli, Structure, physical and thermal properties of WO_3-GeO_2-TeO_2 glasses, Mater. Chem. Phys. 121 (2010) 335–341.

[8] K.M. Kaky, G. Lakshminarayana, S.O. Baki, I. V Kityk, Y.H. Taufiq-Yap, M.A. Mahdi, Structural, thermal and optical absorption features of heavy metal oxides doped tellurite rich glasses, Results Phys. 7 (2017) 166–174.

[9] M.N. Garaga, U. Werner-Zwanziger, J.W. Zwanziger, A. DeCeanne, B. Hauke, K. Bozer, S. Feller, Short-range structure of TeO_2 glass, J. Phys. Chem. C 121 (2017) 28117–28124.

[10] N. Elkhoshkhany, R. Essam, others, Influence of La_2O_3 on the structural, optical and thermal properties of TeO_2-ZnO-Li_2O-Nb_2O_5 glass, J. Non-Cryst. Solids 536 (2020) 119994.

[11] L.M.S. El-Deen, M.S. Al Salhi, M.M. Elkholy, IR and UV spectral studies for rare earths-doped tellurite glasses, J. Alloys Compd. 465 (2008) 333–339.

[12] S.S. Babu, P. Babu, C.K. Jayasankar, A.S. Joshi, A. Speghini, M. Bettinelli, Luminescence and optical absorption properties of Nd^{3+} ions in K-Mg-Al phosphate and fluorophosphate glasses, J. Phys. Condens. Matter 18 (2006) 3975.

[13] N.S. Tagiara, D. Palles, E.D. Simandiras, V. Psycharis, A. Kyritsis, E.I. Kamitsos, Synthesis, thermal and structural properties of pure TeO_2 glass and zinc-tellurite glasses, J. Non-Cryst. Solids 457 (2017) 116–125.

[14] T. Sekiya, N. Mochida, A. Ohtsuka, M. Tonokawa, Normal vibrations of two polymorphic forms of TeO_2 crystals and assignments of Raman peaks of pure TeO_2 glass, J. Ceram. Soc. Japan. 97 (1989) 1435–1440.

[15] M.R. Sahar, K. Sulhadi, M.S. Rohani, Spectroscopic studies of TeO_2-ZnO-Er_2O_3 glass system, J. Mater. Sci. 42 (2007) 824–827.

[16] N. Mochida, K. Takahashi, K. Nakata, S. Shibusawa, Properties and structure of the binary tellurite glasses containing mono-and di-valent cations, J. Ceram. Assoc. Jpn. 86 (1978) 317–326.

[17] N. Elkhoshkhany, M.A. Khatab, M.A. Kabary, Thermal, FTIR and UV spectral studies on tellurite glasses doped with cerium oxide, Ceram. Int. 44 (2018) 2789–2796.

[18] A. Bachvarova-Nedelcheva, R. Iordanova, S. Ganev, Y. Dimitriev, Glass formation and structural studies of glasses in the TeO_2-ZnO-Bi_2O_3-Nb_2O_5 system, J. Non-Cryst. Solids 503 (2019) 224–231.

[19] M. Çelikbilek, A. Erçin Ersundu, S. Aydin, Glass formation and characterization studies in the TeO_2-WO_3-Na_2O system, J. Am. Ceram. Soc. 96 (2013) 1470–1476.

[20] C. Yu, D. He, G. Wang, J. Zhang, L. Hu, Enhancement of up-conversion

luminescence properties in Yb^{3+}/Tm^{3+}/Er^{3+} tri-doped transparent oxyfluoride tellurite glass ceramics, Chin. Optic Lett. 8 (2010) 197–198.

[21] Z. Pan, A. Ueda, R. Mu, S.H. Morgan, Upconversion luminescence in Er^{3+} doped germanate-oxyfluoride and tellurium-germanate-oxyfluoride transparent glass-ceramics, J. Lumin. 126 (2007) 251–256.

[22] D. Tatar, M.L. Öveçouglu, G. Özen, B. Erim, Glass transition and crystallization of 0.8 TeO$_2$ + 0.2 CdF$_2$ glass, J. Eur. Ceram. Soc. 29 (2009) 329–335.

[23] A. Miguel, R. Morea, J. Gonzalo, M.A. Arriandiaga, J. Fernández, R. Balda, Near-infrared emission and upconversion in Er^{3+} doped TeO$_2$-ZnO-ZnF$_2$ glasses, J. Lumin. 140 (2013) 38–44.

[24] H. Doweidar, G. El-Damrawi, M. Abdelghany, Structure and properties of CaF$_2$-B$_2$O$_3$ glasses, J. Mater. Sci. 47 (2012) 4028–4035.

[25] H. Doweidar, G. El-Damrawi, M. Abdelghany, Structure-properties correlations in PbF$_2$-B$_2$O$_3$ glasses, Phys. Chem. Glas. J. Glas. Sci. Technol. Part B. 55 (2014) 121–129.

[26] K. El-Egili, H. Doweidar, R. Ramadan, A. Altawaf, Role of F$^-$ ions in the structure and properties of BaF$_2$-B$_2$O$_3$ glasses, J. Non-Cryst. Solids 449 (2016) 83–93 http://dx.doi.org/10.1016/j.jnoncrysol.2016.07.014.

[27] H. Doweidar, K. El-Egili, R. Ramadan, E. Khalil, Structural studies and properties of CdF$_2$-B$_2$O$_3$ glasses, J. Non-Cryst. Solids 481 (2018) 494–502.

[28] I.A. Sokolov, V.N. Naraev, A.N. Nosakin, A.A. Pronkin, Influence of MeF$_2$ (Me = Mg, Ca, Sr, and Ba) on the electrical properties of glasses in the MeF$_2$-Na$_2$B$_4$O$_7$ system, glas. Phys. Chem. 26 (2000) 383–389.

[29] E.F. El Agammy, H. Doweidar, K. El-Egili, R. Ramadan, Structure of PbF$_2$–TeO$_2$ glasses and glass-ceramics, Mater. Res. Technol. Accepted (2020), https://doi.org/10.1016/j.jmrt.2020.02.028.

[30] Y.M. Moustafa, K. El-Egili, Infrared spectra of sodium phosphate glasses, J. Non-Cryst. Solids 240 (1998) 144–153.

[31] Y.M. Moustafa, H. Doweidar, G. El-Damrawi, Utilisation of infrared spectroscopy to determine the fraction of the four coordinated borons in borate glasses, Phys. Chem. Glasses 35 (1994) 104–106.

[32] S. Neov, I. Gerasimova, V. Kozhukharov, M. Marinov, The structure of glasses in the TeO$_2$-P$_2$O$_5$ system, J. Mater. Sci. 15 (1980) 1153–1166.

[33] G. Liao, Q. Chen, J. Xing, H. Gebavi, D. Milanese, M. Fokine, M. Ferraris, Preparation and characterization of new fluorotellurite glasses for photonics application, J. Non-Cryst. Solids 355 (2009) 447–452.

[34] Web elements periodic table of elements, http://www.webelements.com.

[35] J.M. Rojo, J. Sanz, J.M. Reau, B. Tanguy, Influence of ion distribution on the ionic conductivity of lithium tellurite glasses (Li$_2$O-TeO$_2$ and LiF-TeO$_2$), J. Non-Cryst. Solids 116 (1990) 167–174.

[36] S. Sakida, S. Hayakawa, T. Yoko, Part 2.^{125}Te NMR study of M$_2$O-TeO$_2$ (M = Li, Na, K, Rb and Cs) glasses, J. Non-Cryst. Solids 243 (1999) 13–25.

[37] T. Sekiya, N. Mochida, A. Ohtsuka, M. Tonokawa, Raman spectra of MO$_{1/2}$-TeO$_2$ (M = Li, Na, K, Rb, Cs and Tl) glasses, J. Non-Cryst. Solids 144 (1992) 128–144.

[38] J. Heo, D. Lam, G.H. Sigel Jr., E.A. Mendoza, D.A. Hensley, Spectroscopic analysis of the structure and properties of alkali tellurite glasses, J. Am. Ceram. Soc. 75 (1992) 277–281.

[39] D. Tatar, G. Özen, F.B. Erim, M.L. Öveçoğlu, Raman characterizations and structural properties of the binary TeO$_2$-WO$_3$, TeO$_2$-CdF$_2$ and ternary TeO$_2$-CdF$_2$-WO$_3$ glasses, J. Raman Spectrosc. 41 (2010) 797–807.

[40] M.D. O'Donnell, C.A. Miller, D. Furniss, V.K. Tikhomirov, A.B. Seddon, Fluorotellurite glasses with improved mid-infrared transmission, J. Non-Cryst. Solids 331 (2003) 48–57.

[41] V. Nazabal, S. Todoroki, S. Inoue, T. Matsumoto, S. Suehara, T. Hondo, T. Araki, T. Cardinal, Spectral properties of Er^{3+} doped oxyfluoride tellurite glasses, J. Non-Cryst. Solids 326 (2003) 359–363.

[42] H. Doweidar, K. El-Egili, G. El-Damrawi, R.M. Ramadan, Sites distribution and properties of Al$_2$O$_3$-PbO-B$_2$O$_3$ glasses, Phys. Chem. Glas. J. Glas. Sci. Technol. Part B. 49 (2008) 271–277.

[43] H. Doweidar, Y.B. Saddeek, Effect of La$_2$O$_3$ on the structure of lead borate glasses, J. Non-Cryst. Solids 356 (2010) 1452–1457.

[44] P.G. Pavani, K. Sadhana, V.C. Mouli, Optical, physical and structural studies of boro-zinc tellurite glasses, Phys. B Condens. Matter 406 (2011) 1242–1247.

[45] N. Kaur, A. Khanna, Structural characterization of borotellurite and alumino-bor-otellurite glasses, J. Non-Cryst. Solids 404 (2014) 116–123.

[46] P.G. Pavani, S. Suresh, V.C. Mouli, Studies on boro cadmium tellurite glasses, Opt. Mater. (Amst) 34 (2011) 215–220.

[47] R.C. Lucacel, I.C. Marcus, I. Ardelean, O. Hulpus, Structural studies of copper doped 2TeO$_2$-PbO-Ag$_2$O glass by FT-IR and Raman spectroscopies, Eur. Phys. J. Appl. Phys. 51 (2010).

[48] T. Sekiya, T. Sekiya, N. Mochida, A. Oshtsuka, M. Tonokawa, J. Non-Cryst. Solids 144 (1992) 128 J. Non-Cryst. Solids. 144 (1992) 128.

[49] P. Charton, P. Armand, Glasses in the TeO$_2$-Sb$_2$O$_4$ binary system, J. Non-Cryst. Solids 316 (2003) 189–197.

[50] P. Armand, P. Charton, New ternary tellurite glasses: TeO$_2$-WO$_3$-Sb$_2$O$_4$ and TeO$_2$-WO$_3$-Ga$_2$O$_3$, Phys. Chem. Glasses 43 (2002) 291–295.

[51] T. Sekiya, N. Mochida, A. Soejima, Raman spectra of binary tellurite glasses containing tri-or tetra-valent cations, J. Non-Cryst. Solids 191 (1995) 115–123.

[52] R.C. Lucacel, I. Ardelean, Comparative structural investigation of B$_2$O$_3$-MO-CuO glasses (MO→ TeO$_2$ or As$_2$O$_3$) by FTIR and Raman spectroscopies, J. Optoelectron. Adv. Mater. 8 (2006) 1124.

[53] M. Tatsumisago, S.-K. Lee, T. Minami, Y. Kowada, Raman spectra of TeO$_2$-based glasses and glassy liquids: local structure change with temperature in relation to fragility of liquid, J. Non-Cryst. Solids 177 (1994) 154–163.

[54] R. Akagi, K. Handa, N. Ohtori, A.C. Hannon, M. Tatsumisago, N. Umesaki, High-temperature structure of K$_2$O-TeO$_2$ glasses, J. Non-Cryst. Solids 256 (1999) 111–118.

[55] Y. Himei, A. Osaka, T. Nanba, Y. Miura, Coordination change of Te atoms in binary tellurite glasses, J. Non-Cryst. Solids 177 (1994) 164–169.

[56] T. Komatsu, H. Tawarayama, H. Mohri, K. Matusita, Properties and crystallization behaviors of TeO$_2$-LiNbO$_3$ glasses, J. Non-Cryst. Solids 135 (1991) 105–113.

[57] C. Duverger, M. Bouazaoui, S. Turrell, Raman spectroscopic investigations of the effect of the doping metal on the structure of binary tellurium-oxide glasses, J. Non-Cryst. Solids 220 (1997) 169–177.

[58] Y. Guo, M. Li, L. Hu, J. Zhang, Effect of fluorine ions on 2.7 μm emission in Er^{3+}/Nd^{3+} codoped fluorotellurite glass, J. Phys. Chem. 116 (2012) 5571–5576.

[59] J.A. Evans, D.A. Long, The vibrational Raman spectra of some complexes formed between the tetrafluorides of Group VI elements and antimony and arsenic penta-fluorides, J. Chem. Soc. A Inorganic Phys. Theor. (1968) 1688–1694.

[60] T. Yoko, K. Kamiya, K. Tanaka, H. Yamada, S. Sakka, Glass-forming region and structure of oxyhalide tellurite glasses containing LiX (X = F and Br) and Li$_2$O, J. Ceram. Soc. Japan. 97 (1989) 289–294.

[61] D.S. Yakovlev, A.P. Mirgorodskii, A.V. Tulub, B.F. Shchegolev, Nonempirical calculation of linear and nonlinear polarizability of TeO$_2$ based molecular clusters and piezoelectric properties of crystalline tellurium oxide, Optic Spectrosc. 92 (2002) 449–454.